Supporting Information Appendix for

Strong Texturing of Lithium Metal in Batteries

Feifei Shi[1], Allen Pei[1], Arturas Vailionis[2], Jin Xie[1], Bofei Liu[1], Jie Zhao[1], Yongji Gong[1] and Yi Cui[1,3]*

1 Department of Materials Science and Engineering, Stanford University, Stanford, CA 94305, USA.
2 Stanford Nano Shared Facilities, Stanford University, Stanford, CA 94305, USA
3 Stanford Institute for Materials and Energy Sciences, SLAC National Accelerator Laboratory, 2575 Sand Hill Road, Menlo Park, CA 94025, USA.

Correspondence to: yicui@stanford.edu

This file includes:

Materials and Methods

1. Electrochemical Experiments

2032-type coin cells with copper or stainless steel working electrodes and Li foil (Alfa Aesar) counter/reference electrodes were assembled in an argon-filled glove box (MB-200B, Mbraun). A double-stacked commercial separator (Celgard 2325) was used between the two electrodes and 30 μL of electrolyte was added to each side. In order to prevent the effect of crimping pressure on the morphology of lithium morphology, a ring-spacer made of poly-imide was placed between the separator and lithium foil, as shown in Figure S1. The thickness of a single ring-spacer is 125 μm, so multiple ring-spacers can be placed to accommodate different thickness of lithium deposit layer. The electrolyte was 1M $LiPF_6$/ethylene carbonate (EC): diethyl carbonate (DEC) (1:1 v/v) (Novolyte Technologies, BASF). 1,3-dioxolane/1,2-dimethoxyethane (DOL/DME, 1:1 v/v) (Sigma-Aldrich) with 1 M lithium bis(trifluoromethylsulfonyl)imide (LiTFSI) (Sigma-Aldrich) with 1 wt% $LiNO_3$ (Sigma-Aldrich) as an additive was used as the electrolyte. Electrolyte salts were dried at 130˚C for over 24h in Ar atmosphere. Dimethyl carbonate (DMC) (Aldrich, 99.9+%, HPLC grade) was used as rinsing solvent. Galvanostatic deposition was conducted using a battery-testing unit from MTI Instruments. The Cu electrode was discharged to 0 V vs. Li/Li^+ by applying 0.5 mA cm^{-2} current, then charged back to 1 V at -0.5 mA cm^{-2} to initialize SEI formation and remove surface impurities. Then, a fixed amount of charge was passed galvanostatically at different current rates depending on the experiment. All the potentials reported here are referenced to the Li/Li^+ redox couple.

Li-Sulfur full battery assembling:

A three-electrode Swagelok cell is used, due to the reactivity of Cu foil with sulfur, a stainless steel spacer was used as a working electrode and Li foil as reference electrodes. The anolyte was made of DOL/DME 1:1 v/v, 1M LiTFSI, 1 wt% $LiNO_3$. The catholyte was prepared with 2.3g Sulphur powder and 0.46 g lithium sulphide mixed in 16 ml DOL/DME (1:1) electrolyte in a 20 ml vial, followed by addition of 0.5 g lithium nitrate and 2 g Bis(trifluoromethane) sulfonimide lithium salt (LiTFSI). The lithium nitrate

and LiTFSI were heated at 110℃ for two days before use. Then the solution was heated and stirred at 70℃ for 6 h to generate a 5M Li_2S_8 solution.

Li-Oxygen full battery assembling:

A three-electrode Swagelok cell is used, with Cu foil as the working electrode, Li foil as the reference electrode, and Li_2O_2 pasted on Al foil as the counter electrode. The electrolyte was prepared as 1M LiTFSI in tetraethylene glycol dimethyl ether (TEGDME). TEGDME solvent was distilled over dry 4Å molecular sieve prior to use.

2. X-ray diffraction measurement setup

X-ray diffraction (XRD) was performed employing a PANalytical X`Pert Materials Research Diffractometer equipped with a Cu-source in parallel beam geometry. Symmetrical x-ray diffraction scans were collected with line-focus source within the range $20° < 2\theta < 90°$ with a 0.02° step size, and a collection time of 0.5s in all cases. The pole figures were measured using the x-ray source in point-focus mode maintaining 3° intervals of ϕ and ψ motors and collection time of 0.5s per step. The incident X-ray beam was collimated by an x-ray lens and the beam size was limited by the cross-slits to the size of 10 × 10 mm. Due to the large grain sizes of Li metal, the beam spot size was intentionally chosen to be large enough for better statistical results. The total single pole figure collection time was around 3h.

Lithium samples' area was controlled to be ~1cm^2. The samples were placed on glass slides and sealed with polyimide tape. In order to protect Li samples from degradation during the prolonged pole figure measurements, Anton-Paar sample stage was utilized, where a high purity argon was used to purge the measurement chamber. The thickness of all electroplating samples was set to be ~200 μm assuring sufficient signal to noise ratio. After the whole measurement, the surface of Li samples remained shining with no evidence of contamination or beam damage to Li sample. Experiment set-up is shown in Figure S2.

We have also collected a pole figure of the Cu foil substrate (CF-T8G-UN-18, Pred Materials International, Inc.) used as the working electrode for Li deposition, showing no texture; therefore the isotropic polycrystalline Cu current collector does not affect

the Li deposit's texture.

3. Surface Morphology Characterization

After electrochemical treatment, the lithium samples were rinsed in DMC to remove residual electrolyte. The samples were then transferred to a scanning electron microscope (SEM) (JSM-6700F, JEOL) for imaging.

4. Solid Electrolyte Interphase Characterization

XPS analysis was performed on the material surface using Phi 5000 VersaProbe, Ulvac-Phi with Al (Kα) radiation (1486 eV). All samples were sealed in a vacuum transfer vessel inside the glove box (<1ppm O_2, H_2O), and then transferred into the vacuum environment (<10^{-5} pascal) for measurement. Carbon 1s peaks of samples were calibrated. Sulfur 2p peaks were examined in detail. All the binding energies were calibrated with respect to the C1s peak at 284.6 eV. Spin-orbit coupling gives rise to a doublet in the S 2p peak (($2p_{1/2}$−$2p_{3/2}$)) separated by 1.18 eV with a 2/1 intensity ratio.

The FTIR spectra were measured with a Nicolet iS5 FT-IR Spectrometer in a glove box (content of H_2O, O_2 < 1 ppm). All of the samples are rinsed with DMC/DOL and dried inside glovebox before test.

Supplementary Text

1. Current density effect

According to Chazalviel's model, an applied current density leads to an ion concentration gradient—high-current density results in near-zero ion concentration at the negative electrode and the formation of Li dendrites at Sand's time, while low current density leads to a minimal and stable ion concentration gradient and no Li dendrites form in this condition. When the current density is low or the inter-electrode distance L is small, there is in principle no Sand behavior and the concentration variation should be small. Figure S3-5 results clearly indicate that the shape Li deposit does not change, despite the diameter decrease with increasing current density.

2. Calculation of diffusion-limiting current, and the ratio of current density to the diffusion-limiting current

The diffusion-limiting current density for an electrochemical cell with electrode spacing L can be readily calculated for a given electrolyte with salt concentration c_0, ambipolar diffusion coefficient D, and anion transference number t_a. Here we have neglected the reduction in ionic conductivity from the separator and assumed there is no convection in the cell

$$J_{\text{limiting}} = \frac{2ec_0D}{t_aL}$$

In Table S1, we have listed literature values of D and t_a for two electrolytes used in this study, 1M $LiPF_6$ in EC/DEC (1:1 v/v) and 1 M LiTFSI in DOL/DME (1:1 v/v), and calculated the limiting current density for each electrolyte in a coin cell with electrode spacing of 50 μm. In some cases, the diffusion coefficient is calculated from ionic conductivity values by using the Einstein relation (D = μkT). To emphasize that standard battery cycling conditions are far from diffusion-limited conditions, we then further compared commonly-used current densities to the limiting current densities. The J_{limiting} for each table is calculated using the combination of D and t_a that gives the lowest value of J_{limiting}. Note that even a relatively high current density of 5 mA/cm^2 is nearly 2 orders of magnitude below the limiting current density.

3. Measurement of exchange current density and interphase resistance

Microelectrodes were homemade using tungsten (W) wire of diameter 25 μm embedded within borosilicate glass. The glass was melted carefully onto the wire such that no gas was trapped between the W wire and the insulating glass layer [10-12]. The end of the electrode was polished before every experiment using a 0.1 μm diamond lapping disc. The resulting electrode geometry is an embedded circular microdisk in glass with electrode area 4.9x10^{-6} cm^2.

Exchange current densities were measured by running cyclic voltammetry scans with the W microelectrode serving as the working electrode and a large Li foil serving as the counter and reference electrode (Figure S8). Due to the low nominal currents (nA-μA),

the polarization of the Li foil is extremely low and it can be considered a reliable reference. The tafel region was fit linearly, and the crossover point was used to find the exchange current density of the Li/Li+ couple in each electrolyte without influence from the SEI.

Symmetric cells were constructed from two lithium metal foil disks with area 1 cm^2 sandwiching an electrolyte-impregnated separator. The electrolytes tested are the standard DOL/DME and EC/DEC electrolytes mentioned previously in the methods section. Additives of 100 ppm water was added to plain electrolyte and used as-is as well. Electrochemical impedance spectroscopy was used to determine the interphase resistance between Li and electrolyte (Figure S9). Table S2 lists the average interphase resistance for 2 cells. In the case for 1 μM Li_2S_8 additives in DOL/DME electrolyte with 1% wt. $LiNO_3$, a galvanic polarization test [9, 13] was conducted instead of an AC impedance test due to the contributions from the redox of polysulfide species. A fixed current, ranging from -50 to +50 μA/cm^2, was applied to a Li-Li symmetric cell, with each current applied for 30 minutes, starting with +10 μA/cm^2, then -10 μA/cm^2, +20 μA/cm^2, etc. The average overpotential was recorded and plotted. The slope of the line is the interphase resistance for the cell in Ohms. Parallel impedance measurements of bulk Li metal in the same electrolytes gave interphase resistances that did not follow the same trends as the exchange current density via SEI-free microelectrode measurements. We found that the interphase resistances in EC/DEC were between 1 and 2 orders of magnitude larger than those in ether-based electrolyte. In contrast, the exchange current densities of the Li/Li^+ reaction with no SEI influence in both types of electrolytes were within the same order of magnitude. The significantly lower interphase resistance for ether-based SEIs is mainly due to the lower dielectric constant of ether-based solvents and the thinner associated SEI thickness. We thus find that lower resistance from the SEI layer does not necessarily manifest as a low exchange current density and hence a more controllable Li deposition. Thus, the fast, primary adsorption of additives/solvents at the Li surface plays a more dominant role in Li crystallization than the following later-formed SEI layer.

References:

1. Lee, S.-I. *et al.* A study of electrochemical kinetics of lithium ion in organic electrolytes. *Korean J. Chem. Eng.* **19,** 638–644 (2002).
2. Lundgren, H., Behm, M. & Lindbergh, G. Electrochemical characterization and temperature dependency of mass-transport properties of $LiPF_6$ in EC:DEC. *J. Electrochem. Soc.* **162,** A413–A420 (2014).
3. Valøen, L. O. & Reimers, J. N. Transport properties of $LiPF_6$-based Li-Ion battery electrolytes. *J. Electrochem. Soc.* **152,** A882 (2005).
4. Kaempgen, M., Chan, C. K., Ma, J., Cui, Y. & Gruner, G. Printable thin film supercapacitors using single-walled carbon nanotubes. *Nano Lett.* **9,** 1872–1876 (2009).
5. Cao, R. *et al.* Effect of the anion activity on the stability of Li metal anodes in lithium-sulfur batteries. *Adv. Funct. Mater.* **26,** 3059–3066 (2016).
6. Kim, H.-S. & Jeong, C.-S. Electrochemical properties of binary electrolytes for lithium-sulfur batteries. *Bull. Korean Chem. Soc.* **32,** 3682–3686 (2011).
7. Safari, M., Kwok, C. Y. & Nazar, L. F. Transport properties of polysulfide species in lithium–sulfur battery electrolytes: coupling of experiment and theory. *ACS Cent. Sci.* **2,** 560–568 (2016).
8. Suo, L. *et al.* A new class of solvent-in-salt electrolyte for high-energy rechargeable metallic lithium batteries. *Nat. Commun.* **4,** 1481 (2013).
9. Munichandraiah, N., Scanlon, L.G., Marsh, R.A., Kumar, B., Sircar, A.K. Determination of the exchange current density of the $Li^+ + e^- = Li$ reaction in polymer electrolytes by galvanostatic linear polarization of symmetrical cells *J. Electroanal. Chem.* **179,** 495-499 (1994).
10. Pletcher, D., Rohan, J. F., Ritchie, A. G., Microelectrode studies of the lithium/proplyene carbonate system-part I. electrode reactions at potentials positive to lithium deposition *Electrochim. Acta*, **39**. 1369-1376 (1994)
11 Pletcher, D., Rohan, J. F., Ritchie, A. G., Microelectrode studies of the lithium/proplyene carbonate system-part II. studies of bulk lithium deposition and dissolution *Electrochim. Acta*, **39**. 2015-2023, (1994)

12 Aojula, K. S., Genders, J. D., Holding, A. D., Pletcher, D., Application of microelectrodes to the study of the Li/Li^+ couple in ether solvents-III *Electrochim. Acta*, **34**. 1535-1539, (1989)

13. Fana, F. Y. *et al.* Solvent Effects on Polysulfide Redox Kinetics and Ionic Conductivity in Lithium-Sulfur Batteries. *J. Electrochem. Soc.* **163,** A3111-A3116 (2016).

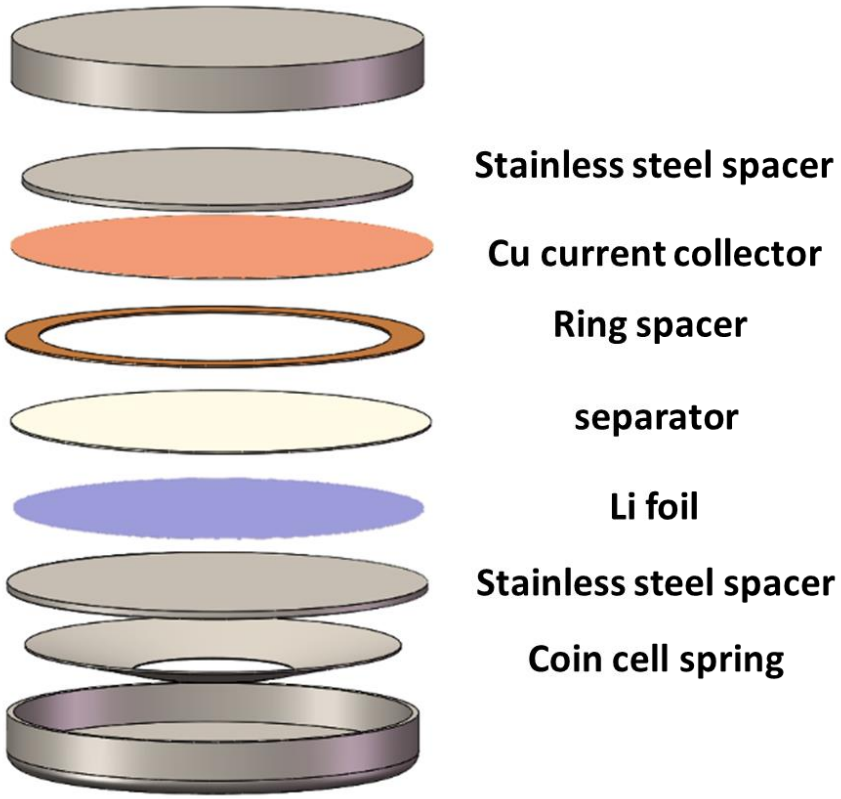

Figure S1. Details of coin-cell set-up

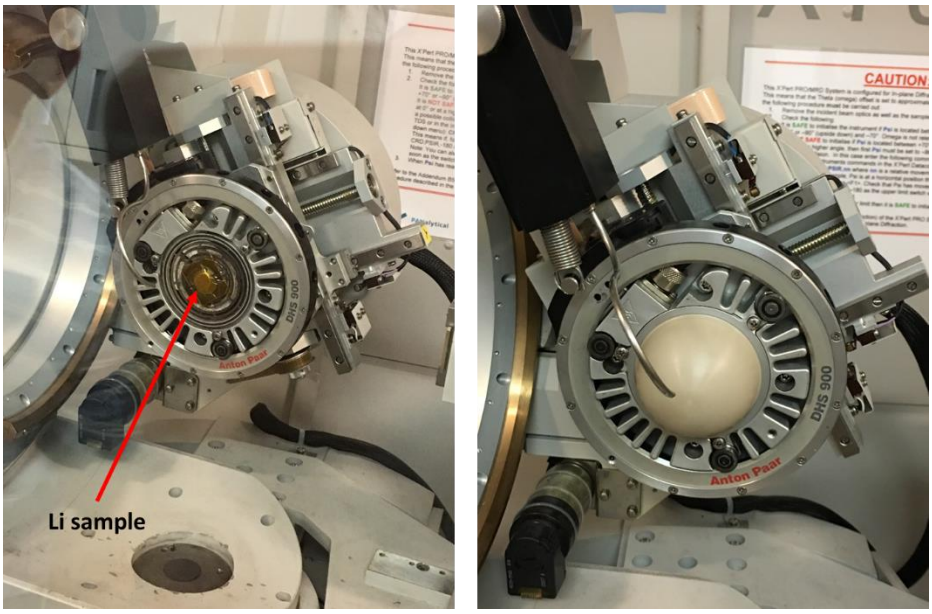

Figure S2. Experiment set-up of X-ray diffraction measurement

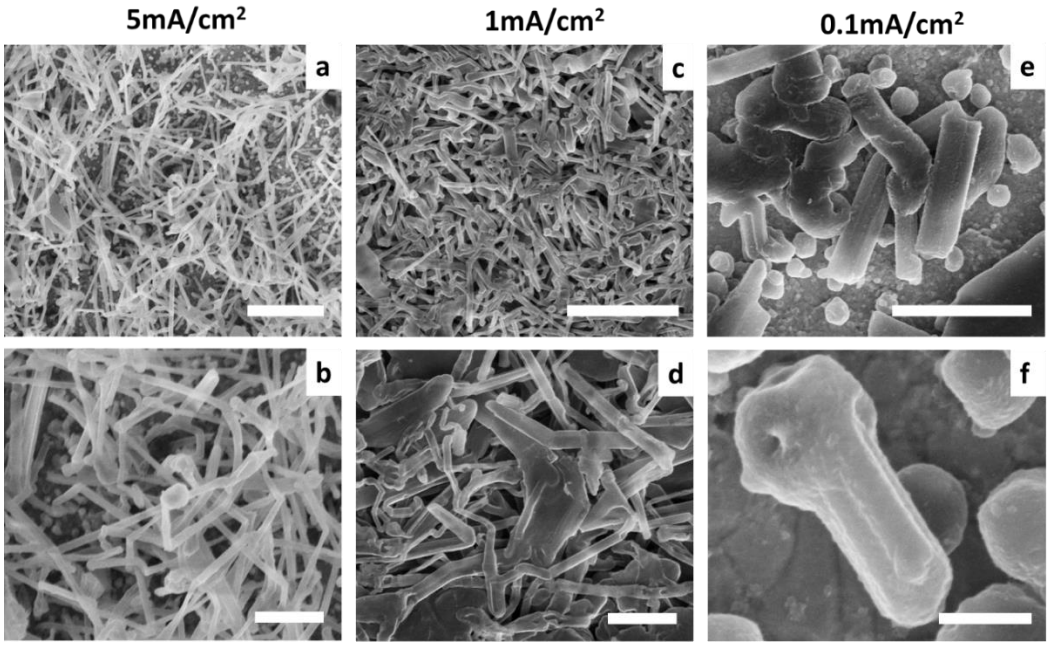

Figure S3. Lithium deposition morphology in EC/DEC 1M $LiPF_6$ electrolyte systems at various current density of (a, b) 5 mA/cm^2, (c, d) 1 mA/cm^2, (e, f) 0.1 mA/cm^2, with lithium deposition capacity of 1 mAh/cm^2. The scale bars in (a, c, e) are 5 μm, in (b, d,) are 2 μm, in (f) is 1 μm.

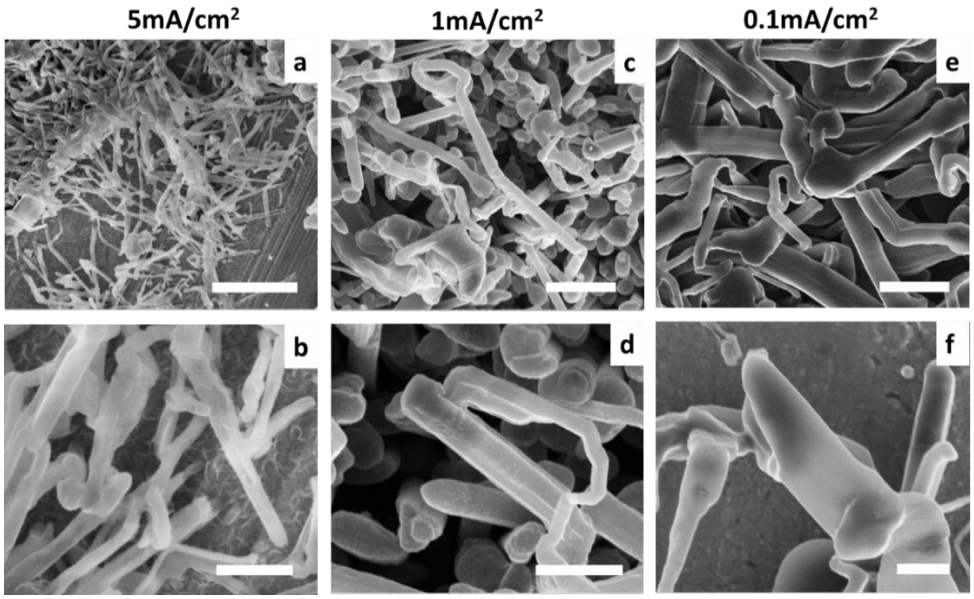

Figure S4. Lithium deposition morphology in DOL/DME 1M LiTFSI without $LiNO_3$ electrolyte systems at various current density of (a, b) 5 mA/cm^2, (c, d) 1 mA/cm^2, (e, f) 0.1 mA/cm^2, 1 mAh/cm^2. The scale bars in (a, c, e) are 5 μm, in (b) is 1 μm in (d, f) are 2 μm.

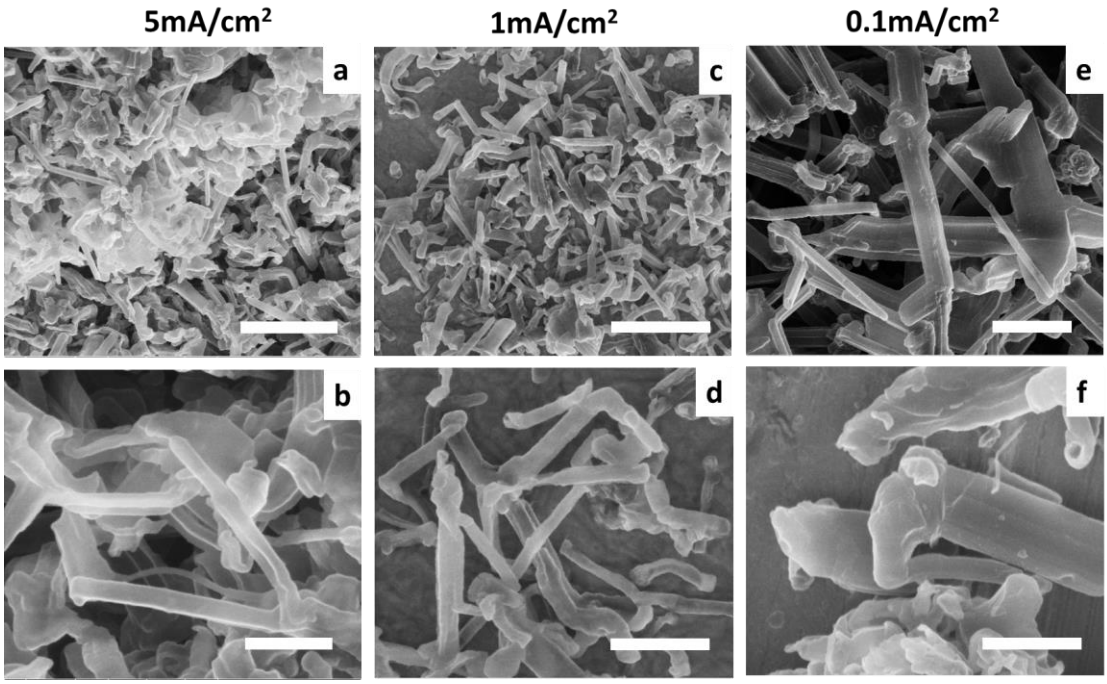

Figure S5. Lithium deposition morphology in TEGDME 1M LiTFSI electrolyte systems at various current density of (a, b) 5 mA/cm^2, (c, d) 1 mA/cm^2 , (e, f) 0.1 mA/cm^2, 1 mAh/cm^2. The scale bars in (a, c, e) are 5 µm, in (b) is 1 µm in (d, f) are 2 µm.

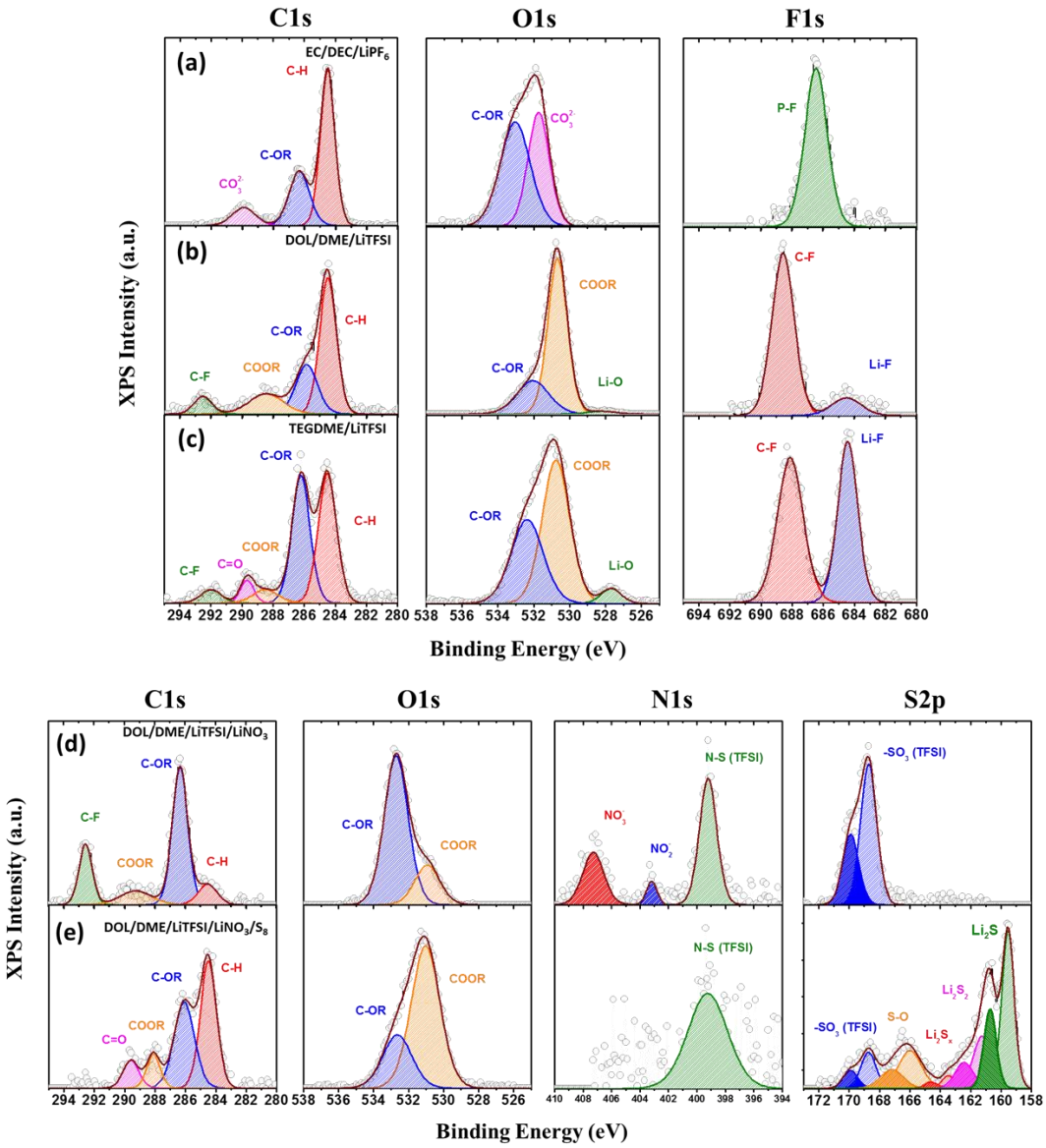

Figure S6. XPS spectra of SEI on Lithium deposits prepared in (a) EC/DEC 1M $LiPF_6$ (b) DOL/DME 1M LiTFSI, (c) TEGDME 1M LiTFSI, (d) DOL/DME 1M LiTFSI, 1% $LiNO_3$, (e) sulfur catholyte 5M S_8 dissolved in DOL/DME 1M LiTFSI, 1% $LiNO_3$. All of the sample preparations are done inside an Ar glovebox and a vacuum transfer vessel is used during the transfer between Ar glovebox (<1 ppm O_2, H_2O) and ultra-high vacuum environment ($<10^{-5}$ pascal).

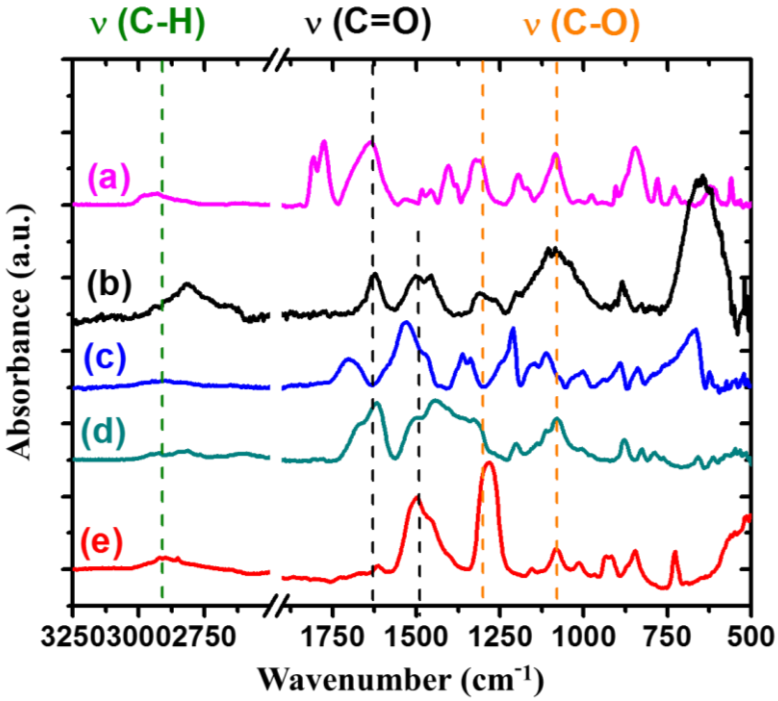

Figure S7. FTIR spectra of SEI on Lithium deposits prepared in (a) EC/DEC 1M $LiPF_6$ (b) DOL/DME 1M LiTFSI , (c) TEGDME 1M LiTFSI, (d) DOL/DME 1M LiTFSI, 1% $LiNO_3$ and (e) sulfur catholyte 5M S_8 dissolved in DOL/DME 1M LiTFSI, 1% $LiNO_3$. All of the sample preparations and measurements are done under Ar inside glovebox.

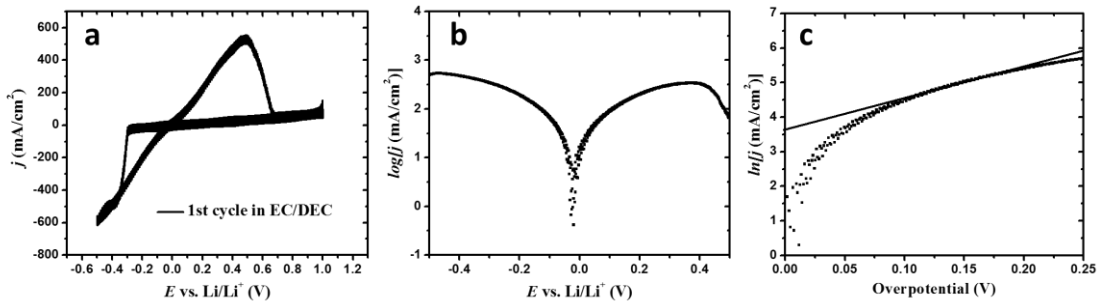

Figure S8. (a) Cyclic voltammetry for 25 μm microelectrode in EC/DEC electrolyte, sweep rate, 200 mV/s. (b) log plot of current density versus voltage (c) Tafel slope fitting used to calculate exchange current densities. All of exchange current density in various electrolytes are summarized in Table 2.

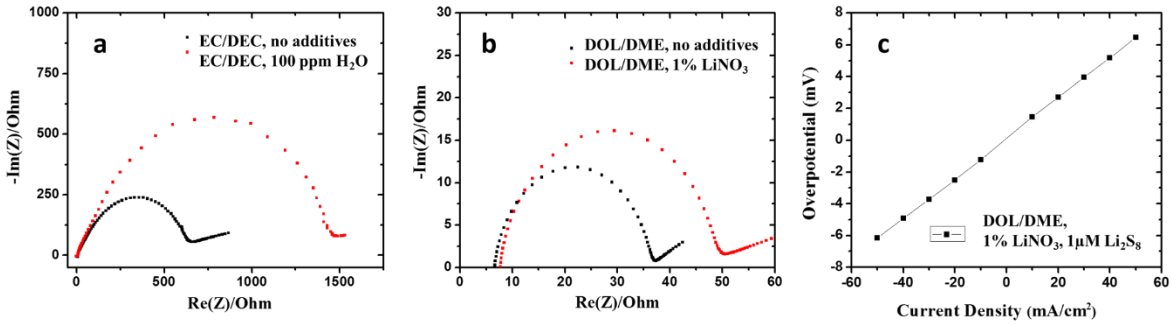

Figure S9. Electrochemical impedance spectroscopy for Li-Li symmetric cells with **(a)** EC/DEC-based electrolytes with and without 100 ppm H_2O. **(b)**DOL/DME-based electrolytes with and without 1% wt. $LiNO_3$ additives. **(c)** Plot of overpotential vs. current density for a Li-Li symmetric cell with DOL/DME-based electrolyte with 1% wt. $LiNO_3$ and 1 μM polysulfide additives. Data taken from galvanostatic polarization tests.

Table S1. Values of lithium ion diffusion coefficient, anion transference number, and calculated diffusion-limiting current densities for common electrolytes.

Electrolyte	$\mathbf{D_{Li+}}$[cm^2/s]	t_a	**Ref.**	$J_{limiting}$ [mA/cm^2]	$J / J_{limiting}$ [%]		
					0.1 mA/cm^2	1.0 mA/cm^2	5.0 mA/cm^2
1 M $LiPF_6$ EC/DEC (1:1 v/v)	1.5 $x10^{-6}$ – 2.66 $x10^{-6}$	0.2 - 0.38	1-4	152	0.066%	0.66%	3.3%
1 M LiTFSI DOL/DME (1:1 v/v)	2.93 $x10^{-6}$ – 5.33 $x10^{-6}$	0.47 - 0.57	5-9	198	0.051%	0.51%	2.5%

Table S2. Exchange current densities and Interphase resistance for Li surfaces in various carbonate-based and ether-based electrolytes. (All values an average of 2 cells)

Electrolyte	1 M $LiPF_6$ EC/DEC	1 M $LiPF_6$ EC/DEC 100 ppm H_2O	1 M LiTFSI DOL/DME	1 M LiTFSI DOL/DME 1% $LiNO_3$	1 M LiTFSI DOL/DME 1% $LiNO_3$ 1 μM Li_2S_8
Exchange current density, j_0, [mA/cm^2]	35	28	123	27	25
Interphase resistance, R [Ω]	702	1374	35.6	38.3	127